NJC

Accepted Manuscript

This is an *Accepted Manuscript*, which has been through the Royal Society of Chemistry peer review process and has been accepted for publication.

Accepted Manuscripts are published online shortly after acceptance, before technical editing, formatting and proof reading. Using this free service, authors can make their results available to the community, in citable form, before we publish the edited article. We will replace this *Accepted Manuscript* with the edited and formatted *Advance Article* as soon as it is available.

You can find more information about *Accepted Manuscripts* in the Information for Authors.

Please note that technical editing may introduce minor changes to the text and/or graphics, which may alter content. The journal's standard Terms & Conditions and the Ethical guidelines still apply. In no event shall the Royal Society of Chemistry be held responsible for any errors or omissions in this *Accepted Manuscript* or any consequences arising from the use of any information it contains.

ROYAL SOCIETY OF CHEMISTRY

www.rsc.org/njc

NJC

ARTICLE

Physical Properties Exploration of Highly Oriented V_2O_5 Thin Films Prepared by Electron Beam Evaporation

Received 00th January 20xx,
Accepted 00th January 20xx

DOI: 10.1039/x0xx00000x

www.rsc.org/

Shrividhya Thiagarajan[a], Mahalingam Thaiyan[b] and Ravi Ganesan[a*]

Highly oriented vanadium pentoxide (V_2O_5) thin films were grown by electron beam (EB) evaporation on glass substrates at 473 K. V_2O_5 thin films were coated with various thicknesses (≈800-1200 nm) by varying the distance from the source and substrates. Influence of film thickness on its physical properties were deeply studied by various characterization techniques. XRD studies were performed to investigate the structural confirmation and preferential lattice orientation of EB evaporated films. Voigt profile method was used to estimate the microstructural parameters and elaborately discussed its dependency of film thickness. SEM micrographs perceived that the prepared films were nearly homogeneous with densely packed morphology. AFM topographical images depicted that the nanograins on the surface of the films. Raman spectra confirmed the formation of α-V_2O_5 polymorph without secondary phase formation. From the optical absorption data, the indirect optical band gap 'E_g' was found to be 2.36 eV for higher thickness V_2O_5 thin film. Optical constants such as refractive index (n), extinction coefficient (k), optical conductivity (σ) and dielectric constants (ε) were evaluated using an approximation protocol developed from well recognized procedures using the data obtained from UV-Vis spectroscopic technique. The luminescence properties variations was observed by photoluminescence (PL) spectroscopy and it has elucidated that the film thickness role on the EB evaporated V_2O_5 films. The Hall mobility and carrier density were found to increase with film thickness.

Introduction

Transition metal oxides are of great interest because of their wide range of peculiar optical [1], transport [2] and magnetic properties [3] which remain incompletely understood. Strongly correlated transitional metal oxide system exhibiting metal to insulator transition (MIT) is explored in recent past as a fundamental functional materials [4]. Among them MIT and Mott-Hubbard behavior of vanadium oxide system which occurs above room temperature (340 K) has attracted many researchers and is investigated in recent past [5]. V_2O_5 has many unusual properties owing to its rich oxidation states (V^{2+} to V^{5+}) and its coordination geometries yielding remarkable structural arrangements [6]. It finds wide range of applications in thermochromic devices like thermal regulators, IR detectors, tagging and labeling due to its negative differential thermal emittance and hence it is demonstrated as naturally disordered meta material by Mikhail et al [7]. The existence of VO_5 octahedral coordination geometry makes it a suitable intercalation/deintercalation host for lighter elements. This gives them reversible and persistent optical, electronic and structural properties that can be employed in electrochromic devices and Li/Na based energy storage devices [8-13]. Dietze et al have illustrated the feasibility of using VO_2 as potential candidate for photoconductive devices [14]. Apart from these, V_2O_5 finds applications in sensors [15], actuators [16], magnetic applications [17] and fiber optic devices [18]. Furthermore, tuning of thickness, morphology and particle size has pronounced effect in altering properties of any material due to enhanced surface to volume ratio and dimension [19]. 2D confinement of materials, only not yields good property but also gives possibility for miniaturization of devices [20]. Several methods were used for the preparation of V_2O_5 thin films such as spray pyrolysis [21], RF sputtering [22], electrodeposition[23], pulsed laser deposition [24], chemical methods [25], thermal evaporation [26] etc. Among them, electron beam – physical vapor deposition (EB-PVD) yields high quality, uniform and large scale deposition suitable for constructing device prototypes for various applications in research and industries.

In the present work, V_2O_5 thin films were deposited by electron beam physical vapor evaporation method at various thicknesses from ≈800 to ≈1200 nm. Various probing tools like Raman spectroscopy, X-ray diffractometer, scanning electron microscopy, atomic force microscopy, energy dispersive spectroscopy, photoluminescence spectroscopy, UV-Vis spectroscopy and Hall measurements were used to analyze and understand the influence of thickness on the structural, optical, morphological, compositional, luminescence and transport properties of V_2O_5 thin films at room temperature.

Experimental

The vanadium pentoxide (V_2O_5) thin films were deposited by electron beam evaporation technique. Well etched glass substrates were ultrasonically cleaned using isopropyl alcohol for 30 minutes.

[a]School of Physics, Alagappa University, Karaikudi, India-630004
E-mail: gravicrc@gmail.com; raviganesa@rediffmail.com
Telephone: +91-04565-225206; Fax: +91-04565-225202
[b]Department of Electrical and Computer Engineering, Ajou University, South Korea, Suwon 443749
Electronic Supplementary Information (ESI) available: [details of any supplementary information available should be included here]. See DOI: 10.1039/x0xx00000x

The pelletized V_2O_5 (purity > 99.99%) were taken in graphite crucibles, kept on water-cooled copper hearth of the electron gun, inside the vacuum chamber. The chamber was evacuated to a high vacuum of the order of 10^{-5} mbar using rotary and diffusion pumps. In the electron gun, the electrons were extracted from a dc heated cathode of tungsten filament, by the application of electric field which pass through an anode and deflected through an angle of about 180° by the magnetic field and reach the target material. The surface of V_2O_5 pellet was scanned by the resultant and deflected electron beam with an accelerating voltage of 5 kV. The vapor phase of the evaporated material were condensed and deposited as thin film layer on the surface of the substrates. The vertical distance was fixed as 12 cm from the source, while the substrates were placed at different horizontal distances from the source to vary the thickness of the films. The detailed substrate position variations are provided in the schematic diagram of **fig.1(a)**. Substrate temperature (T_S) was maintained at 473 K throughout all depositions[27].

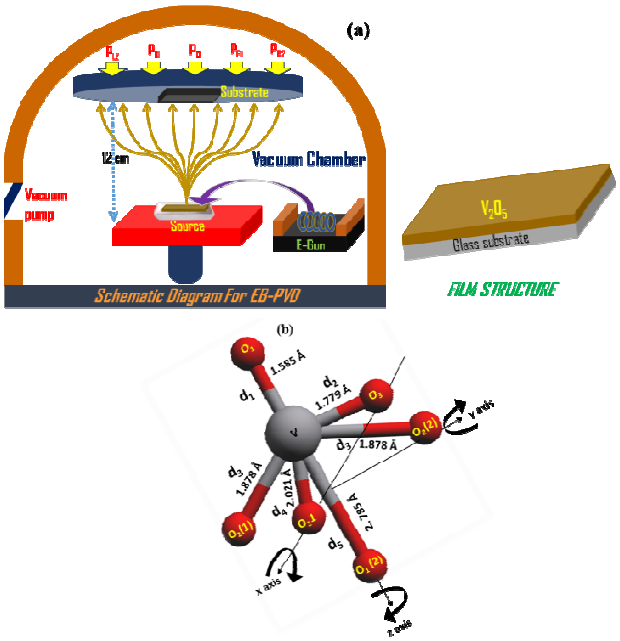

Fig. 1(a) Schematic diagram for EB-PVD deposition and the substrate position for V_2O_5 thin films preparation. The substrate positional variation is obviously enlightened in the schematic; (b) Geometrical 3D view of V_2O_5 structure with the characteristic interatomic distances

Thickness of the deposited V_2O_5 thin films were measured using a stylus profilometer (Mitutoyo SJ-301) equipped with diamond needle. Micro-Raman spectra were collected using Princeton Acton SP 2500 instrument with 0.5 focal length grating monochromator. Raman scattering measurements were performed using 514.5 nm excitation line from Ar^+ laser. X-ray diffractograms were recorded using X'PERT PRO Panalytical diffractometer using Cu-K_α ($\lambda = 0.154$ nm) as source radiation over the range 10-80°. Morphological analyses were performed using FEI QUANTA scanning electron microscope (SEM). Atomic force microscope (AFM) analysis was used for topographical studies. The optical properties were studied using UV-Vis spectrophotometer (PERKIN ELMER LAMDA 9) over the range of 400-1500 nm. Luminescence properties were demonstrated using Cary Eclipse fluorescence spectrophotometer using 330 nm Xe laser as excitation source at room temperature. Hall effect measurements were carried out using ECOPIA HMS-3000 using Van Der Pauw method to comprehend the room temperature transport properties of V_2O_5 thin films deposited at different thickness.

Results and discussion

(a) Structural studies

V_2O_5 thin films were deposited onto glass substrates with various thicknesses by placing the substrate at different distances from the target using electron beam-physical vapor deposition method. The horizontal distance from the center of the source to the substrate position was varied in both directions and named position as P_0 (center), P_{R1} (4 cm to right side), P_{R2} (8 cm to right side), P_{L1} (4 cm to left side) and P_{L2} (8 cm to left side). The detailed schematic diagram is presented in **fig. 1(a)** to reveal the substrate positions in the experiment. In **fig. 1(b)**, the crystal structure is depicted by the geometrical diagram with its characteristics interatomic distance [28]. V_2O_5 belongs to the orthorhombic structure with Pmmn space group symmetry and D_{2h} point group with the lattice constants $a = 11.51$ Å, $b = 3.56$ Å and $c = 4.37$ Å [JCPDS Card No # 41-1426]. The vanadium atom and the three inequivalent oxygen positions O_3 (bridge), O_1 (vanadyl) and O_2 (chain) are shown together with the bonds between the vanadium and the nearest neighbouring oxygen atoms. The linear chain oxygen atoms are linked together with vanadium atoms in the y direction. In the x direction, the vanadium atoms are connected by the bridge oxygen atoms. The bond length of vanadium and oxygen atoms are 1.779 Å (V-O_3), 1.878 Å (V-O_2(2)) and 2.021 Å (V-O_2(1)). The vanadyl oxygens are positioned above and below the vanadium atoms creating the shortest (1.585 Å) and longest (2.785 Å) vanadium-oxygen distances in this structure along the z direction. This structure can be defined as a ladder structure with the legs running along y and the rungs along x described by Atzkern et al [29]. Each vanadium atom and its five nearest oxygen neighbours create VO_5 pyramids which share their corners within the ladder and their edges between neighbouring ladders. The resulting layers are stacked along the c direction. We would like to remark that actually the vanadium is shifted out of the base plane of the pyramid toward the vanadyl oxygen [29]. The film thickness analysis is performed by a stylus profilometer. The measured thickness are ≈840, ≈910, ≈998, ≈1100 and ≈1200 nm for the relative substrate positions of P_{R2}, P_{L2}, P_{R1}, P_{L1} and P_0, respectively. Ad-atoms nearer to the electron gun source are expected to gain more kinetic energy than that is farther. The surface diffusion of these ad-atoms with the momentum transfer sets off nucleation and growth of V_2O_5 thin films onto the substrate surface. This growth kinetics results in reduced thickness while moving away from the source [30]. The film thickness plays a prominent role in the microstructural and electrical properties of V_2O_5 matrix.

Raman spectroscopy is known to be a very useful tool for monitoring the structural order–disorder degree at short range and crystallinity of oxide materials. There are 14 atoms per unit cell and hence 42 degrees of freedom corresponding to zone-center modes [31]. Baddour et al., demonstrated 3 translational (zero frequencies) and 39 vibrational (optical) irreducible representations using group symmetry analysis. Among them 15 belongs to IR active phonon modes and remaining 21 corresponds to Raman active phonon modes [32]. **Fig. 2** depicts the micro-Raman spectra of V_2O_5 thin films with various thicknesses deposited at substrate temperature 473 K (T_S). From the Raman spectra, the prepared film can be assigned to the specific signature of α-V_2O_5 polymorph [33]. The peaks are at lower frequency range of 500-100 cm^{-1} which is hard to predict due to the coupling effect. However, all the frequencies are attributed to the corresponding modes of vibrations as a supporting information in the table S1, which are in good agreement with the earlier reports[12, 23, 34, 35].No other peaks representing secondary phases of vanadium and oxygen were observed that ascertains single phase formation. Also, the absence of peak at 850 cm^{-1} indicated that the films are not hydrated ($V_2O_5.H_2O$) normally observed in V_2O_5[36]. The enhanced peak intensity and broadening with increase of film

thickness manifests the decrease of crystallite size which may be due to lattice-phonon confinement effect [37].

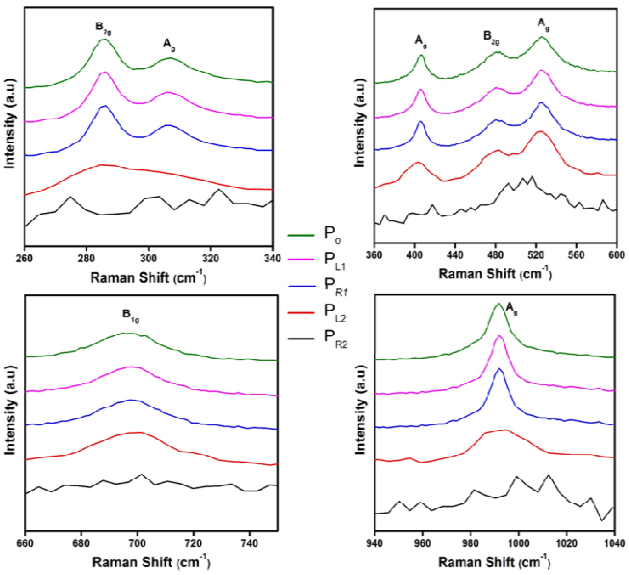

Fig. 2 Raman spectra of V_2O_5 thin films prepared at different thicknesses. (a) The stretching mode V=O related B_{2g} and intra ladder oxygen atoms related A_g Raman shift is exhibited. In the lower thickness (800 nm) exhibited film does not emit the Raman peak. Also, 900 nm thickness film exhibits solely displayed V=O related B_{2g} peak with lower intensity. The B_{2g} and A_g Raman shift intensity and broadening are increased with increase of film thickness; (b) The stretching mode V=O related A_g Raman shift is observed and its intensity linearly increases with thickness. The bending vibration of V–O–V related B_{2g} bond (d_2) and stretching vibration of V-O-V bridging A_g bond (d_4) are displayed at 483 and 525 cm^{-1}, respectively; (c) Asymmetric bond stretching mode of V-O-V bridging B_{1g} bond (d_3)is exhibited at 701 cm^{-1}; (d) The stretching mode vanadium connected oxygen atoms (V=O) A_g bond (d_1) observed at 996 cm^{-1} whose intensity increased linearly with the film thickness.

Fig.3(a) shows XRD patterns of V_2O_5 thin films deposited at various thicknesses. It reveals crystalline thin films with orthorhombic structure. The observed XRD reflections at an angle 20.26° and 41.4° corresponding to the lattice orientation of (001) and (002) planes respectively, which is in good agreement with the JCPDS card No # 41-1426. The deposited film seems to be single lattice orientation up to 1000 nm thickness of the film and (002) reflection plane is exhibited for beyond the thickness value of 1000 nm. From this observation, the higher film thickness encourages polycrystalline nature of film and also increases the crystallinity. It is believed that the high mobility of ad-atom enhances the crystallinity of thin films. It is worthy to note that thin films are highly oriented along the (001) preferential plane perpendicular to c-axis. Lakshmi et al., suggested that such orientations is very useful for intercalation of hosts for Li ions, like in rechargeable batteries and electrochromic devices [38]. The peak broadening of (001) lattice orientation is given in **fig. 3(b)**. The broadening of the peak is obviously increased with increase of film thickness. This broadening also increases the full-width at half maximum (FWHM) values of the film. In this FWHM values are given the prominent role to evaluate microstructural properties of prepared V_2O_5 thin films.

Microstructural parameters were evaluated using Voigt profile method [39]. The structural studies depicted the overall influence of film thickness on the crystalline nature of V_2O_5 thin films. Debye-Scherer's [39] formula using full-width at half-maximum intensity (FWHM) expressed in radians as

$$D = \frac{0.9\lambda}{\beta \cos\theta} \quad (1)$$

where D is crystallite size and β is the FWHM. The crystallite size can be precisely altered by varying the substrate position on the substrate holder as given in schematic diagram. The microstrain 'ε' is evaluated from the equation (2)[39]

$$\frac{\beta\cos\theta}{\lambda} = \frac{1}{D} + \frac{\varepsilon \sin\theta}{\lambda} \quad (2)$$

where 'λ' is the wavelength of X-ray, 'D' is the crystallite size, 'β' the FWHM of the predominant orientation and 'θ' is Bragg's angle respectively. The dislocation density 'δ' [39] can be defined as the length of dislocation lines per unit volume of the crystal and to be determined from the crystallite size 'D' by the relation:

$$\delta = \frac{n}{D^2} \quad (3)$$

where 'n' is a factor, when equal to unity gives minimum dislocation density. The number of crystallites/unit area [39] is calculated using the formula

$$N = \frac{t}{D^3} \quad (4)$$

where 't' is a thickness of the film. The texture coefficient [39] is calculated from the formula,

$$T_C(hkl) = \frac{I(hkl)/I_o(hkl)}{N^{-1}\sum_{n=1}^{N} I(hkl)/I_o(hkl)} \quad (5)$$

where I(hkl) is the measured relative intensity of a plane (hkl), I_o(hkl) is the standard relative intensity of the plane (hkl) taken from the JCPDS card, N is the number of reflections.

Stacking fault probability was calculated from the formula,

$$\alpha = \left(\frac{2\Pi^2}{45\sqrt{3}}\right)\left[\frac{\Delta(2\theta)}{\tan\theta}\right] \quad (6)$$

Table 1 shows the variation of microstructural parameters such as crystallite size, microstrain, dislocation density and number of crystallites for V_2O_5 thin films. The crystallite sizes of V_2O_5 thin films are linearly decreased with increase of film thickness. The crystallite size values are found to be 31, 35, 40 and 45 nm for ≈1200, ≈1100, ≈1000 and ≈900 nm thickness V_2O_5 thin films, respectively. The crystallite size decreases with increase of film thickness is due to the quantum confinement effect. The lattice imperfection nature could be decreased due to the crystallite size decrement [40]. The evaluated microstrain values are inversely proportional to the crystallite size of the films. This may due to an enhancement of internal microstrain with decrease in crystallite size of the films. The maximum value of microstrain is obtained at 0.025 $lines^{-2}m^{-4}$ for V_2O_5 thin film deposited at P_0 position. An aggregate of distorted crystallites as a measure of the crystallite size and strain could affect the variance of the X-ray diffraction line profiles. It is evident from table 1, the dislocation density values are increased with increase of film thickness. This behavior might be due to increase of microstrain with film thickness enhancement. The maximum value of dislocation density is estimated as 1.01 x 10^{15} $lines/m^2$ for V_2O_5 thin film deposited at P_0 position. The decrease of crystallite size is attributed to the increase of the grain boundaries and the amount of defects in the crystalline structure. The increase of dislocation density (δ) values indicated that the enrichment of dislocation defect in the structure. The number of crystallites value is increased with the increase of thickness due to the detraction of crystallite size as given in the table 1. The substrate

position highly dominates the deposition rate by the absorption of vaporized particles from the source. The change is stacking fault probability is plotted as a function of thickness in **fig. S1**. It may be noted that the stacking fault probability reduces with decrease of crystallite size. This manifests reduced defects at higher thickness.

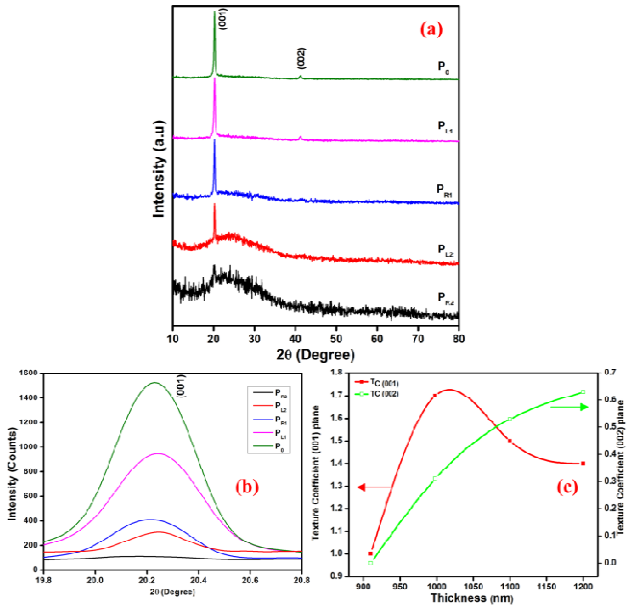

Fig. 3 (a) XRD patterns of V_2O_5 thin films prepared at various thickness by adjusting substrate positions. The lower thickness film reflects amorphous signature in the XRD pattern; (b) Peak broadening in XRD along (001) reflection for V_2O_5 thin films. The peak broadening and intensity of the peak are linearly enhanced with the film thickness; (c) Texture coefficient along (001) and (002) planes.

Table 1 Microstructural parameters of V_2O_5 thin films prepared at different substrate positions

Sample Code	Thickness (nm)± 30 nm	Crystallite Size (nm)	Dislocation Density (× 10^{15} lines/m^2)	Micro strain (lines^{-2} m^{-4})	No of Crystallites per unit area (10^{15} crystallites/m^2)
P_0	1200	31	1.01	0.025	40
P_{L1}	1100	35	0.82	0.022	25
P_{R1}	998	40	0.63	0.020	15
P_{L2}	910	45	0.54	0.017	9
P_{R2}	840	-	-	-	-

The variation in film thickness influences the film stresses induced in the layers. Consequently the dislocation density is increased due to the release of stresses built-up in the layers. The maximum value of strain and dislocations exhibited at higher thickness V_2O_5 thin films improves the stoichiometry in the films, which in turn causes the volumetric expansion of films. The functional dependency of strain and dislocation density and decrease of crystallite size indicates that the alteration of substrate position is the key factor for creating structures of various sizes with limited strain and dislocations. The dislocation density and microstrain values are increased with the film thickness may be due to the strain induced mismatch of thermal expansion coefficient between the material (8×10^{-6}/K) and glass substrate (4.6×10^{-6}/K)[41]. The texture coefficient gives the quantitative information about the preferential crystallite orientation. The texture coefficient along (001) and (002) planes were calculated and plotted in **fig. 3(c)** for V_2O_5 thin films. A sample with randomly oriented crystallite presents T_C (hkl) ≤1, while the high value is an indicator of the larger abundance of crystallites oriented at the particular (hkl) plane. The texture coefficient value of predominant peak (001) is found to be 1.72 for higher film thickness. The increase of thickness might have induced the regular arrangement of atoms in the highly textured V_2O_5 film.

(b) Surface properties

Scanning electron microscopy (SEM) is demonstrated to be a unique and versatile method to analyze morphological properties of V_2O_5 films and also to determine the grain size. **Fig.S2 (a-e)** shows typical SEM micrographs of V_2O_5 thin films deposited at different substrate positions such as P_0, P_{R2}, P_{L2}, P_{R1}, P_{L1} as indicated in schematic diagram. **Fig.S2** shows the smooth surface morphology with the nano-sized grains covered the entire surface of the films. However, films prepared at various substrate positions exhibit strong adherence to the substrates. Also, these films are compact and dense. It is observed that the surface is highly homogenous and is free from pin holes, cracks or voids. No agglomerations are observed on the surface. Such morphology indicates that the films possess good microstructure. The particles are very densely packed and could not be measured from the SEM images. These surface properties have strong effect on the optical properties such as transmittance, absorbance and reflection. There is no other significant variation observed in the SEM micrographs of various thickness prepared V_2O_5 thin films.

Furthermore, the surface topology of V_2O_5 thin films was examined using atomic force microscopy (AFM). **Fig. 4** shows the two-dimensional (2D) and three-dimensional (3D) topographical images of V_2O_5 thin films deposited at various film thicknesses. The amorphous nature topology of the surface is exhibited by lower thickness V_2O_5 thin film prepared at P_{R2} position. Also, at some places presence of patchy type of grains demonstrated the agglomeration process. The displayed AFM images are an obvious evidence to understand surface properties of V_2O_5 films prepared at various thicknesses. The needle shaped crystalline topology of the film is enlightened by 2D and 3D AFM image of V_2O_5 thin film deposited at higher thicknesses by keeping the substrates at P_0 position. 3D images confirmed the grain growth with uniform heights and are highly oriented in particular direction, which is consistent with the XRD and Raman results. The mixture of needle shaped grains with slight amorphous signature is observed in topographical 2D and 3D image of V_2O_5 thin film with ≈ 900 nm thickness deposited at P_{L2} position. This V_2O_5 thin film exhibits higher thickness than the one deposited at P_{R2} position. The nano level grains with pin holes and voids are observed in 2D image of P_{L2}. The smaller grains are joined together to form bunches of grains in the surface of the film. The AFM images are correlated with XRD patterns and also indicate a columnar growth of V_2O_5 films. The highly dense state of topography is observed with an inhomogeneous distribution of grains on the surface as shown in **fig.4**. AFM reveals the granular nature of particles and agglomeration of particles is seen from the 3D micrographs. These images support the SEM data (ESI) revealing tight packing density

(c) Optical and electrical properties

The optical properties of V_2O_5 thin films were analyzed using UV-Vis-NIR spectrometer recorded at room temperature in air. **Fig. 5(a)** represents spectral transmittance as a function of wavelength for V_2O_5 thin films of different thickness measured at normal incidence. The transmittance percentage is decreased from 82 to 60 % in the visible region as film thickness increases. This is associated with the higher packing density of thicker films resulting in higher grain boundary scattering [42].The optical properties dissimilarity might be

highly correlated with the film thickness variation. This finding is consistent with the XRD, Raman and SEM data. The transmittance values rapidly increased in the 410-570 nm wavelength region and thereafter slightly decreased up to 850 nm and saturated for V_2O_5 thin films deposited at P_{L2} and P_{R1} positions. The interference pattern in transmittance spectra are observed for V_2O_5 thin films deposited at higher thickness as shown in **fig. 5(a)**. This nature can be enabled due to the highly homogeneity of the film. The band edge is shifted to the higher wavelength region due to the alteration of film thickness and grain boundaries. The band edge is comparable with the earlier reports of Santos et al[43].

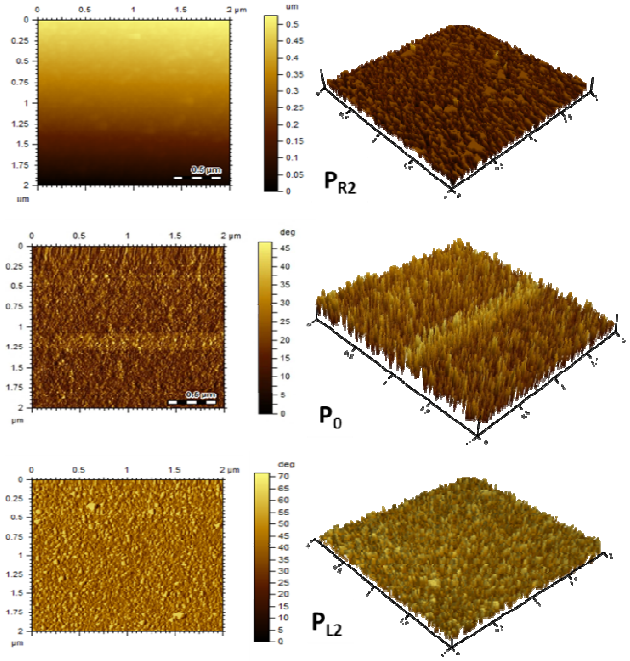

Fig. 4 AFM topographs of V_2O_5 thin films prepared at various thickness by adjusting substrate positions. The amorphous background topograph is envisaged at P_{R2} position prepared V_2O_5 film. The needle like regularly arranged topograph is observed for P_0 position prepared film. The different sizes of grains are observed due to the agglomeration of smaller size grains in the topograph of P_{L2}positionprepared film.

The capability of a material to absorb light is estimated by its absorption coefficient [44]. The band gap value of semiconductors can be evaluated by employing the following equation:

$$\alpha h\nu = K(h\nu - E_g)^n \quad (7)$$

where α is absorption coefficient, hν is the discrete photon energy, K is a constant, E_g is the band gap energy and n depends upon the type of optical transmission in the band gap region. The band gap value is estimated using n=1/2 corresponding to indirect band gap transition. The extrapolation of plot to the *x*-axis gives the band gap energy of V_2O_5 thin film (**Fig. 5(b)**). The energy band gap value of electron beam evaporated V_2O_5 thin film is found to be 2.18-2.36 eV using Tauc's plot. The indirect band gap energy of V_2O_5 thin film is found to be 2.36 eV for higher thickness films and this value is in good agreement with the earlier report [45]. The crystallite size and strain values are given predominant role to shift band gap energy from lower to higher. The crystallinity of V_2O_5 thin films are proven by XRD pattern due to the film thickness alterations. In the present work, the increase in the band gap energy may be attributed to predominant crystallite size reduction and enhancement of strain with enlargement of FWHM at higher film thickness. It is evident that indirect band gap shifts towards higher energy with shrinkage in crystallite size. The band gap is increased from 2.18 to 2.36 eV with corresponding crystallite size reduction of 45 – 31 nm for V_2O_5 thin films deposited at different substrate positions. It is well known that the optical properties of the vanadium pentoxide are strongly affected by the type and concentration of defects in the sample. The enrichment of bandgap with reduction of crystallites size suggested that the surface defects are responsible for the intra-gap states. Furthermore, the experimental transmittance data are used to calculate the optical constants for much strengthen our observation.

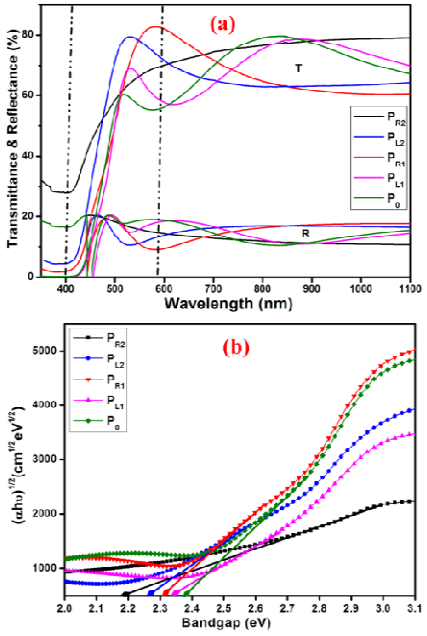

Fig. 5 (a) Transmittance and reflectance spectra of V_2O_5 thin films deposited at different thickness by adjusting substrate positions. The interference pattern in the transmission spectra is elucidated that the highly crystalline nature of film surface; (b) Tauc's plot of V_2O_5 thin films deposited at various film thickness;

Refractive index plays a major role in the fabrication of optoelectronic devices. **Fig. 6(a)** represents the variation of refractive index (*n*) with wavelength for V_2O_5 thin films deposited at different substrate positions. Transmission spectra values are used to estimate the refractive index using a modified algorithm of the envelope method proposed by Swanepoel[46]. It is observed that refractive index values tend to decreases function of wavelength for V_2O_5 thin films. Also, refractive index values are decreased with film thicknesses. The reduction of refractive indices might be due to the close packing nature of the grains as coalescence of grains caused the densification of the layers with increase of film thickness. The extinction coefficient (*k*) V_2O_5 thin films is estimated using an expression reported by Shrividhya et al [42]. **Fig. 6(b)** shows the variation of extinction coefficient of V_2O_5 thin films as a function of wavelength. The extinction coefficient is decreased as increase of V_2O_5 thin film thicknesses which may be due to increase of absorption coefficient [47]. These results suggest that the V_2O_5 films exhibited at normal dispersions in the UV-Vis-NIR region. The earlier reports are in close agreement with our proposed results [48, 49].

The complex dielectric constant variations for V_2O_5 thin films prepared at different substrate position are shown in **fig. S3(a, b).** The imaginary and real parts of the dielectric constant can be designed and it is linearly associated to the density of states within the forbidden gap of the investigated oxides [50]. The real part of dielectric constant decreases with increase in wavelength for all the

prepared V_2O_5 films. The complex dielectric constant values are decreased with increase of film thickness, which may be due to the reduction of grain boundaries thereby changing the structure and morphology of the surface. It has been well established that the complex dielectric constant clamp down as the size of quantum confined physical systems are in the nanometric range. The observation of dielectric suppression might be due to the atomic coordination-number imperfection, which dictates that the size dependence of the atoms orientation and electron-phonon coupling, thus determines the entire band structure such as band gap reduction or expansion. Optical conductivity, which is defined as the transport of photons in a material is one of the powerful tools for studying the electronic states of semiconductors. The optical conductivity of V_2O_5 thin films deposited at various substrate positions as a function of wavelength are estimated using refractive index and absorption coefficient and displayed in the **fig. S3(c)**. The optical conductivity values are originated from the inter band transition due to electron−phonon interaction [51].

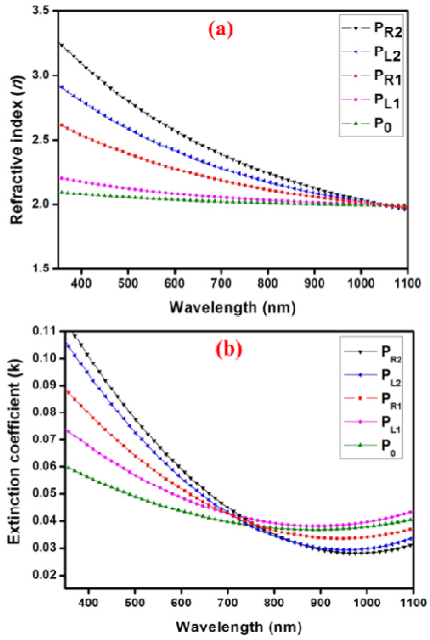

Fig. 6(a) The variation of refractive index as a function of wave length for V_2O_5 thin films with various thickness; (b) The variation of extinction coefficient as a function of wave length for V_2O_5 thin films various thickness

Fig. 7(a) shows photoluminescence (PL) emission spectra at room temperature for V_2O_5 thin films deposited at various thicknesses using an emission wavelength of 258 nm. A wide emission peak is observed at ~485 and 526 nm. The peak broadening and intensity is increased as increase of film thickness which is due to the enrichment behaviour of luminescence properties of V_2O_5. The Gaussian resolved peak position is enlightened in the **fig. 7(b)** for V_2O_5 thin film deposited at P_0 position which yielded maximum film thickness in the present work. The closeness of PL peak position with the absorption edge implied that the luminescence is related to the band edge recombination in V_2O_5 thin films [52, 53]. The peak emission near ~542 nm may be due the recombination of conduction band lowest split-off V-*3d* electron and valence band O-*2p* electron [54]. Interestingly, the emission spectra revealed that the V_2O_5 thin films have exhibited considerable enhancement in the luminescence properties due to variations in film thickness. It is known that the nano level crystallite size generally possess a high-density of surface state. These surface states may act as traps for the photo excited carriers and may suppress excitonic luminescence considerably. This result may be attributed to effective distribution of surface states in V_2O_5 matrix, thereby enhancing the luminescence yield. The luminescence spectra band diagram is provided to represent the dual peak emission (**fig. 7(c)**). The wide range of Gaussian resolved emission peak for lower thickness V_2O_5 thin films is given in **fig. S4(a-d)**.

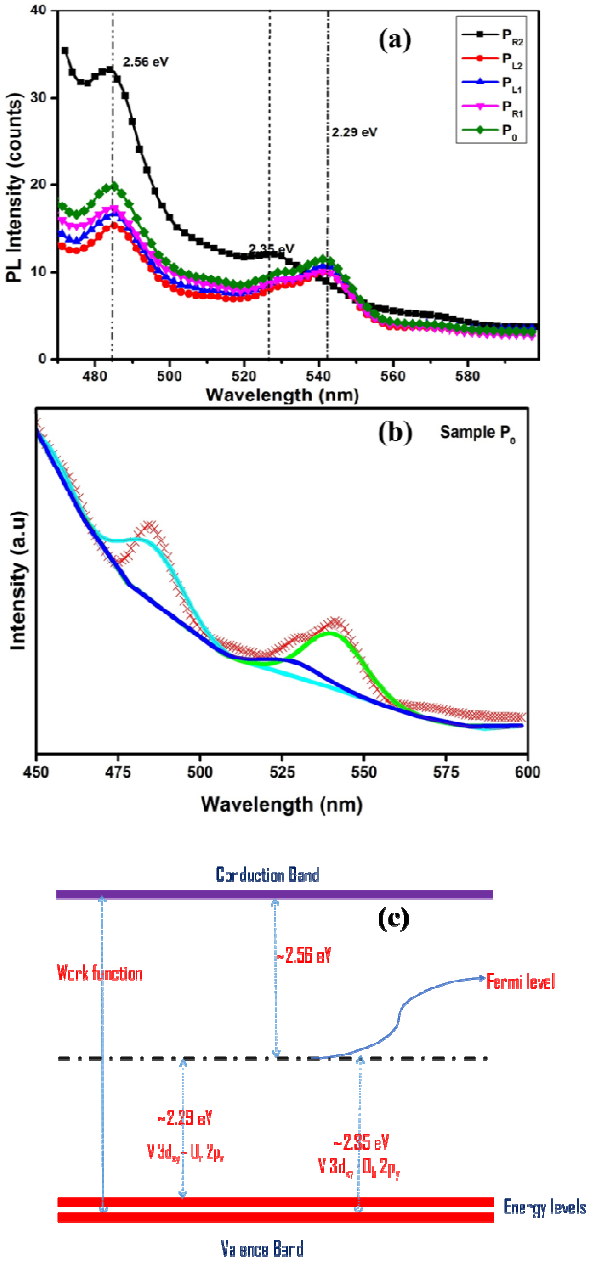

Fig. 7 (a) Photoluminescence spectra of V_2O_5 thin films deposited at different thickness by adjusting substrate positions; (b) Gaussian resolved PL spectra of 1200 nm thick V_2O_5 thin film; (c) The luminescence spectra band diagram for V_2O_5 thin films.

Fig. 8 shows that the electrical transport properties for V_2O_5 thin films measured by van der Pauw Hall measurement. As the film thickness increases, the resistivity decreases and the carrier concentration and mobility of the films are increase. The transport properties of thin film are greatly influenced by their crystallinity[55].

This may lead to enhancement of mobility and carrier concentration with increase of film thickness. Also, the amorphous signatures at lower film thickness contributed to higher resistivity in these films. V_2O_5 thin film with higher thickness has lower resistivity (1011 Ω.cm) and high mobility (496 cm^2/V.s) and carrier concentration (3.202×10^{13} cm^3) compared to other thin films deposited at lower thickness. This is a desired property for electrochromic device [56]. There are very few experimental reports available in literature for RT Hall measurement of V_2O_5 thin films. Abo et al., reported RT Hall measurement for thin films deposited at various substrate temperatures. They showed that the conductivity in V_2O_5 thin films are due to the presence of complex charge transfer mechanism of V^{4+} ions [57]. Manil et al., reported temperature dependent Hall measurement for crystalline and amorphous thin films[58]. The reported higher mobility value than the previous reports is be due to the homogeneous surface nature, lower crystallite size and higher crystallinity at higher thickness prepared V_2O_5 thin film.

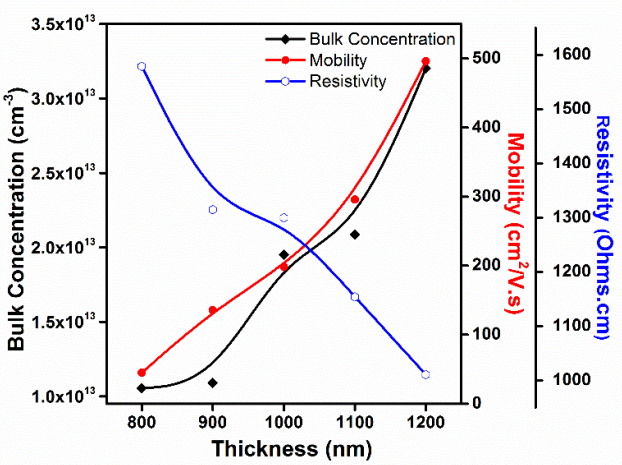

Fig. 8 Room temperature Hall measurement properties variation of V_2O_5 thin films deposited at different thickness by adjusting substrate positions.

Conclusions

We have demonstrated the formation of highly oriented V_2O_5 thin films with an orthorhombic phase using the Electron Beam – Physical Vapour Deposition (EB-PVD) technique. The film thickness was varied by adjusting the substrate position on the substrate holder and the thickness were found to be in the range of 800-1200 nm. The prepared V_2O_5 thin films were crystalline with orientation along (001) lattice plane. XRD and Raman studies were carried out for the structural confirmation of prepared V_2O_5 films. Optical characterization shows that the characteristic transition of semi-conductive indirect band gap energy was lying between 2.18 and 2.36 eV. The optical parameters like refractive index, extinction coefficient, dielectric constant and optical conductivity values were determined from Swanepoel's proposed formulae. Morphological studies revealed that uniform morphology with nano-sized grains were occupied the entire surface of the film. The mobility and carrier concentration values increased with increase of film thickness.V_2O_5 thin films with higher thickness can be optimized and used as a suitable candidate for electrochromic applications.

Acknowledgements

One of the authors, Shrividhya Thiagarajan gratefully acknowledges the UGC-BSR, New Delhi, India for providing financial support.

References

1.C. G. Granqvist, Sol. Energy Mater. and Sol. Cells **99** (0), 1-13 (2012).
2.A. F. Basile, T. Cramer, A. Kyndiah, F. Biscarini and B. Fraboni, J. Appl. Phys. **115** (24), 244504 (2014).
3.S. V. Demishev, A. L. Chernobrovkin, V. V. Glushkov, A. V. Grigorieva, E. A. Goodilin, H. Ohta, S. Okubo, M. Fujisawa, T. Sakurai, N. E. Sluchanko, N. A. Samarin and A. V. Semeno, Phy. Rev. B **84** (9), 094426 (2011).
4.D. Ruzmetov, S. D. Senanayake, V. Narayanamurti and S. Ramanathan, Phy. Rev. B **77** (19), 195442 (2008).
5.M. Imada, A. Fujimori and Y. Tokura, Rev. Mod. Phys. **70** (4), 1039-1263 (1998).
6.J. Yang, T. Lan, J. Liu, Y. Song and M. Wei, Electrochim. Acta **105** (0), 489-495 (2013).
7.M. A. Kats, R. Blanchard, S. Zhang, P. Genevet, C. Ko, S. Ramanathan and F. Capasso, Phy. Rev. X **3** (4), 041004 (2013).
8.A. R. Armstrong, C. Lyness, P. M. Panchmatia, M. S. Islam and P. G. Bruce, Nat Mater **10** (3), 223-229 (2011).
9.X. Chen, E. Pomerantseva, K. Gregorczyk, R. Ghodssi and G. Rubloff, RSC Adv. **3** (13), 4294-4302 (2013).
10.Q. T. Qu, L. L. Liu, Y. P. Wu and R. Holze, Electrochim. Acta **96** (0), 8-12 (2013).
11.V. Raju, J. Rains, C. Gates, W. Luo, X. Wang, W. F. Stickle, G. D. Stucky and X. Ji, Nano Lett. **14** (7), 4119-4124 (2014).
12.H. Yin, C. Song, Y. Wang, S. Li, M. Zeng, Z. Zhang, Z. Zhu and K. Yu, Electrochim. Acta **111** (0), 762-770 (2013).
13.P. Liu, S.-H. Lee, C. E. Tracy and J. A. Turner, J. of Power Sources **119–121** (0), 305-309 (2003).
14.S. H. Dietze, M. J. Marsh, S. Wang, J. G. Ramírez, Z. H. Cai, J. R. Mohanty, I. K. Schuller and O. G. Shpyrko, Phy. Rev. B **90** (16), 165109 (2014).
15.R. R. Andronenko and A. T. Nakusov, Glass Phys. and Chemistry **33** (4), 411-416 (2007).
16.G. Gu, M. Schmid, P.-W. Chiu, A. Minett, J. Fraysse, G.-T. Kim, S. Roth, M. Kozlov, E. Munoz and R. H. Baughman, Nat Mater **2** (5), 316-319 (2003).
17.H. T. Dang and A. J. Millis, Phy. Rev. B **87** (18), 184434 (2013).
18.A. Dhawan, Y. Sharma, L. Brickson and J. F. Muth, Optical Mater. Express **4** (6), 1128-1139 (2014).
19.Y.-F. Sun, S.-B. Liu, F.-L. Meng, J.-Y. Liu, Z. Jin, L.-T. Kong and J.-H. Liu, Sens. **12** (3), 2610-2631 (2012).
20.S. Tokonami, H. Shiigi and T. Nagaoka, Analytica Chimica Acta **641** (1–2), 7-13 (2009).
21.V. Varadaraajan, B. C. Satishkumar, J. Nanda and P. Mohanty, J. of Power Sources **196** (24), 10704-10711 (2011).
22.M. I. Kang, I. K. Kim, E. J. Oh, S. W. Kim, J. W. Ryu and H. Y. Park, Thin Solid Films **520** (6), 2368-2371 (2012).
23.D. Vernardou, E. Spanakis, N. Katsarakis and E. Koudoumas, Adv. Mat. lett. **5** (10), 569-572 (2014).
24.S. Beke, S. Giorgio, L. Kőrösi, L. Nánai and W. Marine, Thin Solid Films **516** (15), 4659-4664 (2008).
25.D. Vernardou, E. Spanakis, G. Kenanakis, E. Koudoumas and N. Katsarakis, Mater. Chem. and Phys. **124** (1), 319-322 (2010).
26.Z. Lu, M. D. Levi, G. Salitra, Y. Gofer, E. Levi and D. Aurbach, J. of electroanal. Chem. **491** (1–2), 211-221 (2000).

27.C. V. Ramana, O. M. Hussain, B. Srinivasulu Naidu, C. Julien and M. Balkanski, Materials Science and Engineering: B **52** (1), 32-39 (1998).
28.H. Bachmann, F. Ahmed and W. Barnes, Z. fur Krist. - Cryst.Mater. **115** (1-6), 110-131 (1961).
29.S. Atzkern, S. V. Borisenko, M. Knupfer, M. S. Golden, J. Fink, A. N. Yaresko, V. N. Antonov, M. Klemm and S. Horn, Phy. Rev. B **61** (19), 12792-12798 (2000).
30.P. M. Martin, (Elseiver Inc., 2010), Vol. 3, pp. 143-145.
31.C. Bhandari and W. R. L. Lambrecht, Phy. Rev. B **89** (4), 045109 (2014).
32.R. Baddour-Hadjean, J. P. Pereira-Ramos, C. Navone and M. Smirnov, Chem. of Mater. **20** (5), 1916-1923 (2008).
33.R. Baddour-Hadjean, M. B. Smirnov, K. S. Smirnov, V. Y. Kazimirov, J. M. Gallardo-Amores, U. Amador, M. E. Arroyo-de Dompablo and J. P. Pereira-Ramos, lnorg. Chem. **51** (5), 3194-3201 (2012).
34.T. Zhai, H. Liu, H. Li, X. Fang, M. Liao, L. Li, H. Zhou, Y. Koide, Y. Bando and D. Golberg, Adv. Mater. **22** (23), 2547-2552 (2010).
35.E. Armstrong, M. Osiak, C. Glynn and C. O'Dwyer, ECS Trans. **58** (14), 3-12 (2014).
36.X. Chen, E. Pomerantseva, P. Banerjee, K. Gregorczyk, R. Ghodssi and G. Rubloff, Chem. of Mater. **24** (7), 1255-1261 (2012).
37.J. Zuo, C. Xu, Y. Liu and Y. Qian, Nanostructured Materials **10** (8), 1331-1335 (1998).
38.B. B. Lakshmi, C. J. Patrissi and C. R. Martin, Chem. of Mater. **9** (11), 2544-2550 (1997).
39.B. D. Cullity, in *Elements of X-ray Diffraction* (Addison-Wesley Publishing Inc, Massachusetts, U.S.A, 1956).
40.Y. Zhang, Z. Yue, Z. Gui and L. Li, Journal of Electroceramics **14** (1), 67-74 (2005).
41.T. N. Kennedy, Hakim, R., McKenzie, J. D., Mater. Res. Bull **2**, 193 (1967).
42.T. Shrividhya, G. Ravi, Y. Hayakawa and T. Mahalingam, J. of Mater. Sci: Mater. in Electron. **25** (9), 3885-3894 (2014).
43.R. Santos, J. Loureiro, A. Nogueira, E. Elangovan, J. V. Pinto, J. P. Veiga, T. Busani, E. Fortunato, R. Martins and I. Ferreira, Appl.Surf.Sci. **282**, 590-594 (2013).
44.V. Dhanasekaran, T. Mahalingam, R. Chandramohan, J.-K. Rhee and J. P. Chu, Thin Solid Films **520** (21), 6608-6613 (2012).
45.A. A. Akl, Appl.Surf.Sci. **252** (24), 8745-8750 (2006).
46.R. Swanepoel, J. of Phys. E: Sci. Instrum. **16** (12), 1214 (1983).
47.V. Dhanasekaran, T. Mahalingam, J.-K. Rhee and J. P. Chu, Opt. - Int. J. of Light and Opt. **124** (3), 255-260 (2013).
48.F. P. Gökdemir, O. Özdemir and K. Kutlu, Electrochim. Acta **121** (0), 240-244 (2014).
49.S. A. Aly, S. A. Mahmoud, N. Z. El-Sayed and M. A. Kaid, Vac. **55** (2), 159-163 (1999).
50.E. Márquez, A. M. Bernal-Oliva, J. M. González-Leal, R. Prieto-Alcón, A. Ledesma, R. Jiménez-Garay and I. Mártil, Mater. Chem. and Phys. **60** (3), 231-239 (1999).
51.P. B. Johnson and R. W. Christy, Phy. Rev. B **9** (12), 5056-5070 (1974).
52.M. Kang, M. Chu, S. W. Kim and J.-W. Ryu, Thin Solid Films **547** (0), 198-201 (2013).
53.M. Kang, E. Oh, I. Kim, S. W. Kim, J.-W. Ryu and Y.-G. Kim, Curr. Appl. Phys. **12** (2), 489-493 (2012).
54.L.-C. Tien and Y.-J. Chen, Appl.Surf.Sci. **258** (8), 3584-3588 (2012).
55.J. W. Orton and M. J. Powell, Reports on Progress in Physics **43** (11), 1263 (1980).
56.C. G. Granqvist, *Handbook of Inorganic Electrochromic Materials*. (Elsevier Science, 1995).
57.A. M. Abo El Soud, B. Mansour and L. I. Soliman, Thin Solid Films **247** (1), 140-143 (1994).
58.M. Kang, J. Jung, S.-Y. Lee, J.-W. Ryu and S. W. Kim, Thermochimica Acta **576** (0), 71-74 (2014).

TABLE OF CONTENTS

GRAPHICAL ABSTRACT

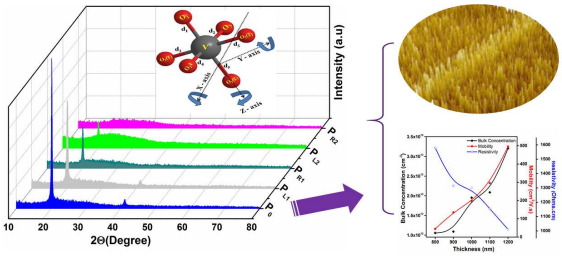

Highly crystalline α-V_2O_5 thin film nanostructures with single phase exhibiting higher mobility was prepared by EB-PVD technique.